

Aspect-ratio-dependent driving force for nonuniform alloying in Stranski-Krastanow islands

D. Digiuni, R. Gatti, and F. Montalenti*

L-NESS and Dipartimento di Scienza dei Materiali, Università degli Studi di Milano-Bicocca, Via R. Cozzi 53, I-20125 Milano, Italy
(Received 13 July 2009; revised manuscript received 22 September 2009; published 16 October 2009)

A semianalytical iterative method for determining the three-dimensional concentration profile minimizing the elastic energy in alloyed heteroepitaxial islands is developed. The method is shown to converge after only a few iterations (solutions of the elastic problem). Exploiting the reduced computational effort, aspect-ratio-dependent and average-concentration-dependent Si/Ge intermixing in alloyed SiGe/Si(001) islands is systematically investigated, considering realistic shapes. Islands providing the better elastic relaxation are also the ones able to lower the elastic load through nonuniform alloying more significantly. Universal behavior in terms of relaxation vs average concentration is demonstrated.

DOI: [10.1103/PhysRevB.80.155436](https://doi.org/10.1103/PhysRevB.80.155436)

PACS number(s): 62.25.-g, 62.23.Eg, 81.40.Jj, 81.10.Aj

I. INTRODUCTION

The Stranski-Krastanow (SK) growth mode is a widely investigated phenomenon characterizing several heteroepitaxial, lattice-mismatched semiconductor systems.^{1,2} In the usual description of SK growth, deposition of a material B on a substrate A causes the formation of a thin wetting layer (WL), followed by three-dimensional islands (3D). The two-dimensional (2D)-3D transition is driven by the attempt to release the elastic energy stored in the WL. Formation of facets, indeed, allows B atoms to partially recover their natural lattice parameter. In the last decade, however, several papers pointed out that SK growth in real systems is more complex: A atoms can indeed be present in the 3D islands causing elastic-energy relaxation to be mediated also by alloying. Even by restricting the attention on two prototypical examples, Ge/Si and InGaAs/GaAs, the literature on the subject is impressive³⁻⁴². This attention is justified by the importance of controlling shape, size, and composition of nanometric islands.^{1,2} In view of possible applications, it is indeed crucial to achieve uniformity in all of the above recalled observables. Moreover, we believe that the challenge posed by the experimental characterization of (rather similar, in the case of Ge/Si) chemical species within nanometer-sized systems further stimulated research work in this field. Impressive results, in terms of 3D compositional maps were obtained both by exploiting x-rays (for recent examples, see Refs. 18, 30, and 40) and selective etching.^{22,27,29,34,39} Interestingly, these studies often revealed nonuniform Ge-concentration profiles.

From the theoretical point of view, qualitatively different approaches have been used to characterize intermixing phenomena. In the first paper pointing out the importance of alloying in SK growth, Tersoff⁴ used a simple continuum model to establish the relative importance of various contributions, including alloying, in 3D island nucleation. A detailed, atomic-scale description of the concentration profiles minimizing the system free energy was obtained by different authors exploiting Monte Carlo (MC) simulations, atom-atom interactions being described by semiempirical potentials.^{17,23,24} The computational cost required by atomistic MC simulations is, however, considerable, preventing one to consider realistically sized islands and/or making it diffi-

cult to gather sufficient statistics at finite temperatures. Models based on elasticity theory solved by finite element methods (FEM) can therefore be extremely helpful. In the MC-FEM method proposed in Refs. 38 and 42, for example, a MC algorithm is used by considering coarse-grained concentration exchanges on a suitable mesh. Alternatively, Medhekar *et al.*³⁶ applied a sequential nonlinear programming method to achieve minimization of the system free energy. Although limited to peculiar (shallow) geometries, it is also worth mentioning the nice work of Ref. 25, yielding analytically the predicted compositional profile for a prepyramidal islands.

In this work, we present a systematic study aimed at understanding the driving force for nonuniform alloying in Ge/Si islands, by finding the Ge distribution $c_{\min}(x,y,z)$ minimizing the elastic energy. A variety of island shapes and average composition values are considered, allowing us to discuss general trends. The paper is organized as follows. In Sec. II a few key results of elasticity theory are recalled, while in Sec. III the recently proposed MC-FEM method^{38,42} is briefly reviewed and updated. In Sec. IV, instead, a faster approach is introduced, successfully tested against MC-FEM, and exploited to produce all results exposed in Sec. V. A general discussion on the importance of determining the concentration profile minimizing the elastic energy is presented in Sec. VI, among with concluding remarks. Although the reader not interested in implementing our methodology can perhaps skip Sec. III, we suggest to follow the derivation of Sec. IV, since it helps following our interpretation of the results.

II. THEORETICAL FRAMEWORK AND NOTATION

In this brief section, we shall recall some basic continuum elasticity theory, and introduce some notation that will be heavily exploited in the remainder of the paper. More details can be found in Ref. 43

An elastic body at equilibrium satisfies the following equation:

$$\begin{cases} -\sigma_{ij,j} = f_i & \text{on } \Omega \\ u_i = 0 & \text{on } \Gamma_D \\ \sigma_{ij}n_j = g_i & \text{on } \Gamma_N \end{cases}, \quad (1)$$

where \mathbf{u} is the displacement field, σ_{ij} the (i,j) component of the stress tensor (which depends on \mathbf{u}), $i(j)=1,2,3$, f_i is the

i -th component of a volumetric force (density) applied to the elastic body, g_i a surface force, Ω the domain occupied by the elastic body, $\Gamma_D \cup \Gamma_N$ its boundary (divided into a sub-boundary Γ_D on which Dirichlet boundary conditions are applied, and a second sub-boundary Γ_N where Neumann boundary conditions are imposed instead), n_j the j -th component of the surface normal to Γ_N , u_i the i -th component of the displacement field. Moreover, the symbol $(\cdot)_{,j}$ is used to indicate the derivative with respect to the j -th coordinate, and summation of repeated indexes is assumed.

For the system treated in this paper, i.e., a SiGe island of variable Ge composition placed on Si, the misfit strain experienced by the island can be conveniently treated as an eigenstrain, thereby following Eshelby formalism for inclusions.⁴⁴ This means solving the homogeneous problem (null volumetric and surface forces, \mathbf{f} and \mathbf{g}) and using the stress-strain relation

$$\sigma_{ij} = \mathcal{C}_{ijkl}(\epsilon_{kl} - \epsilon_{kl}^*), \quad (2)$$

where ϵ^* is the assigned eigenstrain, determining the system reaction minimizing the elastic energy. If the island is made of pure Ge, it will experience a compressive strain, originated by the lattice mismatch, the reaction to which can be mimicked by setting $\epsilon_{ij}^* = \epsilon_m \delta_{ij}$, with $\epsilon_m = 0.04$. If, instead, the Ge fraction $c(x, y, z)$ in the island is neither unitary nor uniform, then $\epsilon_{ij}^* = \epsilon_m c(x, y, z) \delta_{ij}$.

Taking into account the elastic energy due to the eigenstrain ϵ_{ij}^* itself, the total elastic energy can be written as

$$E = \frac{1}{2} \int_{\Omega} dV (\epsilon_{ij} - \epsilon_{ij}^*) \mathcal{C}_{ijkl} (\epsilon_{kl} - \epsilon_{kl}^*). \quad (3)$$

Notice that here and in the following the explicit dependence of several quantities (such as ϵ or c) on the domain point (x, y, z) is omitted to lighten the notation, unless judged as particularly important to follow our discussion.

III. IMPROVED MC-FEM METHOD

The problem of finding the Ge distribution which minimizes the energy of a SiGe island on Si (or the equivalent one for other lattice-mismatched heteroepitaxial systems), for a given average Ge content \bar{c} , can be solved directly by Monte Carlo simulations based on atomistic semiempirical potentials.^{17,23,24} The MC-FEM method was devised to cut the computational cost, through a natural coarse-graining procedure. If in the atomistic approach one exchanges pairs of Si and Ge atoms differently located within the island, accepting the move based on a suitable statistical weight, in MC-FEM somewhat similar exchanges are made between pairs of nodes (α, β) chosen among the mesh on which the elastic problem is solved. For complex three-dimensional geometries requiring a high number of nodes ($\sim 10^4$ or more are typically needed for the systems investigated here) for an accurate numerical solution of Eq. (1), a coarser, *concentration mesh* can be used.³⁸ A schematic illustration is presented in Fig. 1. The concentration in α [$c(\alpha)$] is randomly varied, inducing also a change in $c(\beta)$ since \bar{c} must be kept constant. After each attempted local modification of the Ge concentra-

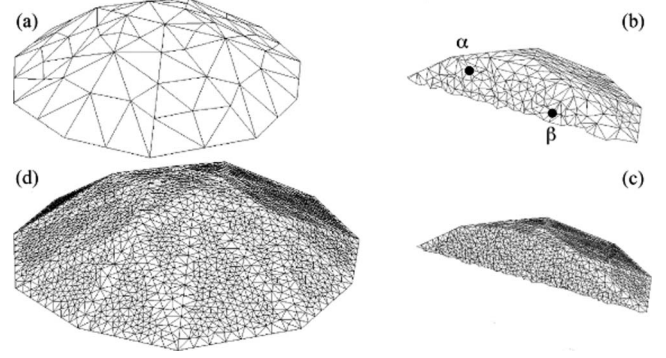


FIG. 1. Typical concentration mesh, with focus on the external (a) and internal (b) nodes. When solving the elastic problem, a much finer mesh (c, d) is used. α and β in panel b represent a possible pair of nodes randomly chosen during the MC-FEM procedure.

tion (from c_{old} to c_{new}), the elastic energy of the system is computed using Eq. (3) with $\epsilon_{ij}^* = c_{\text{new}}(x, y, z) \epsilon_m \delta_{ij}$, while the elastic strain field ϵ is determined using a FEM solver.⁴⁵ If the elastic energy is lowered when passing from c_{old} to c_{new} , the above procedure is repeated starting from c_{new} , iterating until convergence is reached so that the elastic energy is minimized. Applications to free-energy minimization are also possible⁴² but are not discussed in this paper. In MC-FEM, the computational bottleneck is given by calls to the FEM solver. Here, we discuss a rather direct extension allowing for a significant speed-up.

Let us consider a Ge distribution $c_0 = c_0(x, y, z)$, and let E_0 be the associated elastic energy given by Eq. (3), with $\epsilon_{ij}^* = \epsilon_m c_0 \delta_{ij}$. A change $\Delta c = \Delta c(x, y, z)$ in the Ge distribution induces a variation $\Delta \epsilon_{ij}^* = \epsilon_m \Delta c \delta_{ij}$ in the eigenstrain. By exploiting Eq. (3) and neglecting strain relaxation (i.e., by keeping the elastic strain tensor constant), the corresponding energy change is given by

$$\begin{aligned} \Delta E_{\epsilon} &\equiv E_{\epsilon} - E_0 \\ &= \int_{\Omega} dV \left\{ [-\Delta \epsilon_{ij}^* \mathcal{C}_{ijkl} (\epsilon_{kl} - \epsilon_{kl}^*)] + \frac{1}{2} [\Delta \epsilon_{ij}^* \mathcal{C}_{ijkl} \Delta \epsilon_{kl}^*] \right\} \\ &= \int_{\Omega} dV \left\{ [-\epsilon_m \Delta c \delta_{ij} \mathcal{C}_{ijkl} (\epsilon_{kl} - \epsilon_{kl}^*)] \right. \\ &\quad \left. + \frac{1}{2} [\epsilon_m^2 (\Delta c)^2 \delta_{ij} \delta_{kl} \mathcal{C}_{ijkl}] \right\}, \quad (4) \end{aligned}$$

where the subscript ϵ reminds that Eq. (4) yields the energy change at fixed ϵ . Exploiting the relation $\delta_{ij} \mathcal{C}_{ijkl} = A \delta_{kl}$, with $A = (3\lambda + 2\mu)$ for an isotropic material (λ , μ being the Lamé coefficients), and $A = (c_{11} + 2c_{12})$ for a cubic crystal (c_{11} and c_{12} representing the elastic constants), Eq. (4) gives

$$\Delta E_{\epsilon} = -A \epsilon_m \int_{\Omega} \left\{ [\Delta c (\text{Tr } \epsilon - 3 \epsilon_m c_0)] - \frac{3}{2} [\epsilon_m (\Delta c)^2] \right\} dV. \quad (5)$$

Equation (5) can be exploited to find the concentration profile minimizing the elastic energy. The main idea is simple.

Equation (3) provides the elastic energy E . E must be minimized with respect to both the elastic strain ϵ and the load ϵ^* , the latter being determined by the concentration profile. Minimizing ΔE_ϵ using Eq. (5) means performing a line minimization, yielding the optimal Δc for the assigned ϵ . The equivalent minimization at constant ϵ^* can be now performed by solving the elastic problem by FEM, supplying the concentration determined in the previous step. Eq. (5) is then exploited again using the FEM-updated ϵ value, and the whole procedure is iterated until convergence is reached. A straightforward way to exploit Eq. (5) within the MC-FEM scheme is to partially minimize ΔE_ϵ by a sequence of M random concentration changes δc_k , leading to the global change.

$$\Delta c \equiv \sum_{k=1}^M \delta c_k. \quad (6)$$

After combining Eqs. (6) and (5), a few calculations lead to the energy decomposition

$$E_\epsilon = E_0 + \sum_{k=1}^M \delta E_k;$$

$$\delta E_k = -A \epsilon_m \int_{\Omega} dV \left\{ \delta c_k (\text{Tr } \epsilon - 3 \epsilon_m c_{k-1}) - \frac{3}{2} \epsilon_m \delta c_k^2 \right\}, \quad (7)$$

where we have introduced the partial composition profile $c_k \equiv c_0 + \sum_{i=1}^k \delta c_i$. An updated version of the MC-FEM method can be therefore envisaged: M concentration changes lowering the elastic energy at constant strain ϵ (determined by the last call to the FEM solver) are generated, acceptance of the k -th move being determined solely by δE_k in Eq. (7), i.e., without solving the elastic problem. This determines a global change in concentration Δc , and an approximate estimate of the elastic energy E_ϵ . The FEM solver is then called providing the true elastic energy E ($E < E_\epsilon$ since elastic relaxation is added) and strain field ϵ . The procedure is then iterated until the desired concentration profile c_{\min} is found, as sketched in Fig. 2. In Fig. 3, a direct comparison is made between original MC-FEM and the algorithm introduced here, for $M=1$ and $M=10$. In the example, we considered a dome-shaped island modeled as in,⁴⁸ with $\bar{c}=0.5$, and isotropic elastic constants, as derived from the experimental Si (Ge) ones in the substrate (island).⁴⁶ Importantly, all approaches lead to the same result, as illustrated in Fig. 3 in terms of relative elastic-energy relaxation with respect to an island with uniform Ge distribution $c(x,y,z)=\bar{c}$. The resulting concentration profile is shown in the inset of Fig. 3, the physical general meaning being already discussed in.³⁸ As shown in Fig. 3, the improvement guaranteed by exploiting Eq. (7) can be dramatic. For $M=10$, only ~ 200 FEM solutions were needed, corresponding to a decrease of a factor ~ 35 with respect to the original MC-FEM method. For $M=1$, instead, the speed up is only of a factor ~ 3 . It is easy to understand that in this case the cut in computational costs is given by the inverse of the standard MC-FEM acceptance ratio (the FEM solver is called only after a move is accepted). As anticipated, for $M \rightarrow \infty$ the total variation Δc

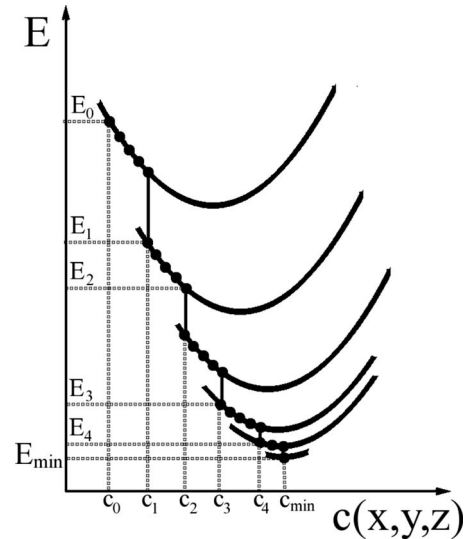


FIG. 2. Scheme representing the improved MC-FEM method. An initial Ge distribution c_0 is chosen, and the elastic problem is solved yielding the elastic energy E_0 and the strain field. At this point, MC concentration changes are performed, by evaluating energy differences based solely on Eq. (7). In the figure, this corresponds to moving along the parabola passing through the point (c_0, E_0) . After M accepted moves lowering the energy ($M=5$ in the figure where each filled circle represent an accepted move), a new concentration distribution c_1 is found. At this stage, the FEM solver is called again, leading to a proper estimate E_1 of the elastic energy (lower than the one found along the parabola). The procedure is iterated until convergence is reached, leading to the Ge distribution $c_{\min}(x,y,z)$ minimizing the elastic energy (E_{\min}).

given by Eq. (6) minimizes the energy functional $E=E(\Delta c)$ in Eq. (5), so that very few FEM calls are predicted to be needed in this case.⁴⁷ We notice, however, that as M increases, the CPU time spent in performing MC exchanges could become comparable with the one spent in solving the

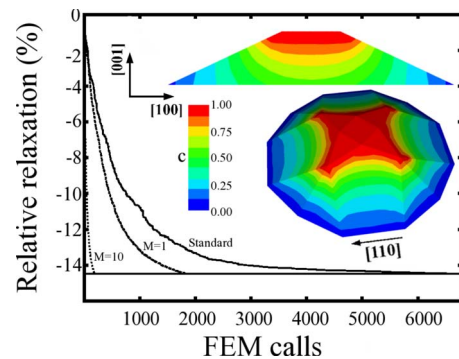


FIG. 3. (Color online) Relative relaxation with respect to the uniform-concentration case as a function of the FEM calls during the iterative procedure. Results refer to a dome-shaped island with an average 50% Ge content. The final concentration profile minimizing the elastic energy (inset, where a top and a perspective view are shown) is found after ~ 7000 FEM calls using standard MC-FEM. Exploiting Eq. (5) and calling the FEM solver only every $M=1$ ($M=10$) accepted moves, ~ 2000 (~ 200) FEM calls are sufficient to reach convergence.

elastic problem. Especially so for problems (typically, complex geometries, and/or several islands) where a high number of nodes are needed in the concentration mesh to provide an accurate description of $c_{\min}(x, y, z)$. Let us now show that the problem can be circumvented by exploiting the simple form of the approximate functional described by Eq. (5).

IV. FAST ALGORITHM FOR ELASTIC-ENERGY MINIMIZATION

Equation (5) gives the energy change ΔE induced by a variation Δc of a given concentration profile c , under the hypothesis that the elastic strain tensor ϵ remains unchanged. Following the discussion reported in the previous section, it is interesting to look for $\Delta c(x, y, z)$ yielding the maximum energy lowering. Since the average composition must be kept constant, the constraint

$$\frac{1}{v} \int_{\Omega} dV \Delta c(x, y, z) = 0 \quad (8)$$

must hold. In Eq. (8), v is the volume of the domain Ω . We then consider the Lagrangian

$$\Delta L = \Delta E(\mathbf{x}) - A \epsilon_m \eta \int_{\Omega} dV \Delta c, \quad (9)$$

where the Lagrange multiplier is chosen to take the form $A \epsilon_m \eta$ in order to make the evaluation easier. Then, we minimize ΔL with respect to Δc and insert the constraint (8). Defining the integral average of the strain tensor trace as $\overline{\text{Tr } \epsilon} \equiv \frac{1}{v} \int_{\Omega} dV \text{Tr } \epsilon$, we find

$$\Delta c = \frac{1}{3 \epsilon_m} (\text{Tr } \epsilon - \overline{\text{Tr } \epsilon}) + (\bar{c} - c). \quad (10)$$

Equation (10) provides the requested Δc analytically, only as a function of known quantities. Using Eq. (10), therefore, allows one to completely skip the MC-based minimization. With the help of Fig. 2, it is easy to understand how an iterative method based on Eq. (10) works. One starts from the initial condition (c_0, E_0) , immediately finds $c_1 = c_0 + \Delta c$ (in Fig. 2, this correspond to jumping in one move to the minimum of the parabola passing through the initial point), calls FEM to update the strain field and the energy value E_1 and iterates the procedure until convergence is reached. A considerable saving in terms of FEM calls is expected since the approximated functional is fully minimized at each step. By applying the method to the very same case treated in the previous section, and leading to the results displayed in Fig. 3, we reached convergence after only ~ 15 FEM calls. While by visually looking at the final concentration profile no differences with the result obtained using the previous methods can be seen (therefore, such profile is not shown), the actual value of the relative lowering in elastic energy shows a small deviation, as it can be seen in Fig. 4. Such deviation is not produced by any particular approximation built in Eq. (10). Simply, in order to make the comparison between different methods very direct we fixed all parameters, including the nodes of the concentration mesh which, in the semianalytical

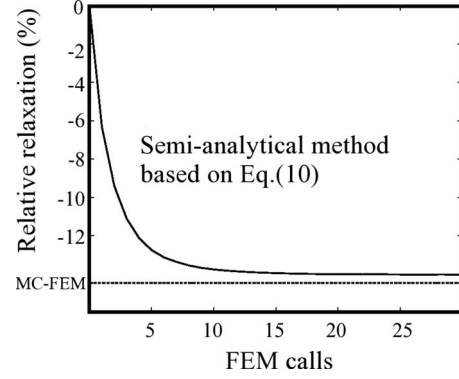


FIG. 4. Relative variation in the elastic energy with respect to the uniform case, as obtained using the semianalytical iterative procedure based on Eq. (10) for the very same system analyzed in Fig. 3. The dashed horizontal line corresponds to the convergent value obtained using standard MC-FEM.

approach, are used to evaluate the strain tensor fixing Δc through Eq. (10). From the numerical point of view, more nodes are needed to yield an accurate description of $\Delta c(x, y, z)$ (semianalytical approach) with respect to the ones simply needed to determine where changes in concentration can occur (MC-based methods). Indeed, by refining the mesh (an operation which requires significant extra computational effort within the MC-based scheme, not in the semianalytical one) we obtained negligible differences with the MC result, without altering significantly the overall efficiency.

By comparing Figs. 4 and 3, it is clear that the semianalytical method allows for a huge reduction in the computational cost required to find the concentration profile minimizing the elastic energy in 3D islands. There is, however, a drawback in the direct use of Eq. (10). The analytical relation leading to the optimal Δc was derived without imposing the physical constraint $0 \leq c(x, y, z) \leq 1$. Within the MC-based procedure, considering such constraint is easy since one can reject moves leading to a violation of the required condition. Eq. (10), instead, leads to a global change in the concentration profile, and some care is needed while treating the problem in case, locally, unphysical $c(x, y, z)$ values are obtained. Actually, for the system considered when generating the results of Figs. 3 and 4 the above problem did not occur. Nonetheless, it would have been sufficient to consider a higher average Ge content and/or a higher aspect-ratio islands to witness the appearance of artificial concentration values, emerging when the system tends to locally segregate Ge (see next section). An easy way to cope with this problem is to split the variation (10) in several small changes. If $c^{(j)}$ is the concentration profiles determined at the j -th step of our iterative procedure, and $\epsilon^{(j)}$ the corresponding strain field, Eq. (10) yields the following concentration at step $j+1$:

$$c^{(j+1)} = c^{(j)} + \frac{1}{3 \epsilon_m} (\text{Tr } \epsilon^{(j)} - \overline{\text{Tr } \epsilon^{(j)}}) + (\bar{c} - c^{(j)}). \quad (11)$$

It is possible to arbitrarily subdivide the total concentration variation between step j and $j+1$ in the following partial changes:

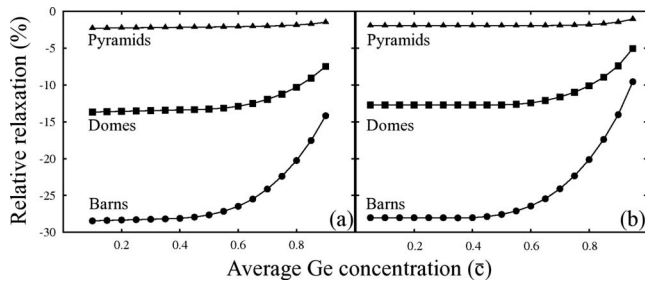


FIG. 5. Relative relaxation with respect to the uniform case produced by nonuniform intermixing minimizing the elastic energy for $\{105\}$ pyramids (triangles), domes (full boxes), and barn-shaped islands (full circles). In panel a, results were obtained by considering \bar{c} -dependent elastic constants, while in panel b, pure-Ge ones were used.

$$c^{(j,k+1)} = c^{(j,k)} + \Gamma \left[\frac{1}{3\epsilon_m} (\text{Tr } \epsilon^{(j)} - \overline{\text{Tr } \epsilon^{(j)}}) + (\bar{c} - c^{(j,k)}) \right], \quad (12)$$

where $c^{(j,0)} \equiv c^{(j)}$, and Γ is a parameter. By assuming that $c^{(j,k)}$ converges as $k \rightarrow \infty$ to some distribution $c^{(j,\infty)}$, we see that

$$\frac{1}{3\epsilon_m} (\text{Tr } \epsilon^{(j)} - \overline{\text{Tr } \epsilon^{(j)}}) + (\bar{c} - c^{(j,\infty)}) = 0, \quad (13)$$

which, compared with Eq. (10), yields $c^{(j,\infty)} = c^{(j+1)}$, i.e., the desired final distribution. The regularization procedure works as follows. We fix a small (positive) Γ value, so that the concentration profile is changed at each step k by very small amounts. If at a step \tilde{k} the partial concentration $c^{(j,\tilde{k})}(x,y,z)$ becomes negative (larger than 1), we fix $c^{(j,\tilde{k})}(x,y,z) = 0$ ($c^{(j,\tilde{k})}(x,y,z) = 1$) for any $k > \tilde{k}$. We directly verified that for $\Gamma \leq 10^{-2}$ the procedure always converge to a $c^{(j,\infty)}(x,y,z)$ profile independent of Γ . Very importantly, we verified that, at the end of the whole iterative procedure (loop over j and k), the predicted $c_{\min}(x,y,z)$ is in full agreement with the MC-based one.

Let us now apply our fast semianalytical method to realistically shaped SiGe islands.

V. RESULTS

In Fig. 5, the behavior of the three main islands observed in Ge/Si heteroepitaxy, i.e., $\{105\}$ pyramids (height to base aspect ratio: A.R.=0.1), domes (A.R. ~ 0.2) and barns (A.R. ~ 0.3 , see Ref. 48 where the geometry of the island is shown) is compared. Once again we focus on the extra relaxation allowed for by nonuniform intermixing. Before commenting the emerging behavior, it is worth to discuss the dependence of the results on the elastic constants. If in the previous sections, being the aim simply to test the method, we considered pure-Ge, isotropic elastic constants within the island, here we shall always use anisotropic, cubic constants. Moreover, results presented in Fig. 5(a) were obtained using \bar{c} -dependent elastic constants, corresponding to ideal $\text{Ge}_{\bar{c}}\text{Si}_{(1-\bar{c})}$ alloys and obtained by linear interpolation.⁵⁰ In

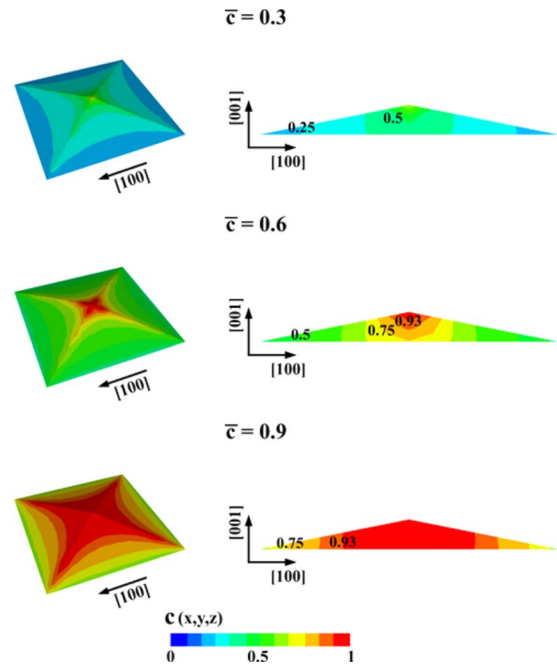


FIG. 6. (Color online) Distribution of Ge minimizing the elastic energy within a $\{105\}$ pyramid with average Ge content $\bar{c}=0.3$ (left and right panel at the top), $\bar{c}=0.6$ (central), and $\bar{c}=0.9$ (bottom). Here and in the following three figures, a few concentration values are explicitly reported to make the plot clearer if printed in black and white.

Fig. 5(b), instead, pure-Ge (anisotropic) constants were used. Overall, it is clear that results depend very weakly on the particular choice (a somewhat larger change is found when comparing isotropic and anisotropic constants. For the $\bar{c}=0.5$ dome case, for example, isotropic calculations lead to an overestimate of $\sim 2\%$ in the relative relaxation). From Fig. 5, it is evident that the higher is the aspect ratio the stronger is the driving force, in terms of elastic-energy reduction, for nonuniform alloying following $c_{\min}(x,y,z)$. Since in the uniform-concentration case the higher is the A.R. the stronger is the elastic relaxation with respect to a flat wetting layer,⁴⁹ we conclude that energy minimization via Ge redistribution further broadens the volumetric-energy gap between shallow and steep islands. The second interesting observation comes from the actual shape of the three curves. In all cases there exists a range of \bar{c} values where the relative relaxation is independent of \bar{c} , pointing out a universal behavior which calls for a deeper analysis. Notice that curves in Fig. 5(a) are never exactly flat, at variance with Fig. 5(b). This is evidently an effect of the \bar{c} -dependent elastic constants. In the following discussion we shall neglect this small effect, ruining the otherwise perfect universal behavior. Along the same lines, all forthcoming figures were obtained by using pure-Ge elastic constants.

In Figs. 6–8 we report $c_{\min}(x,y,z)$ for pyramids, domes, and barns, respectively. From Fig. 6, we see that for $\bar{c}=0.3$ energy minimization induces the formation of a 50%-rich Ge core, extending from the top to the bottom of the island, while a concentration lower than \bar{c} is found at the base of the island. At $\bar{c}=0.6$, the Ge content at the top is raised to

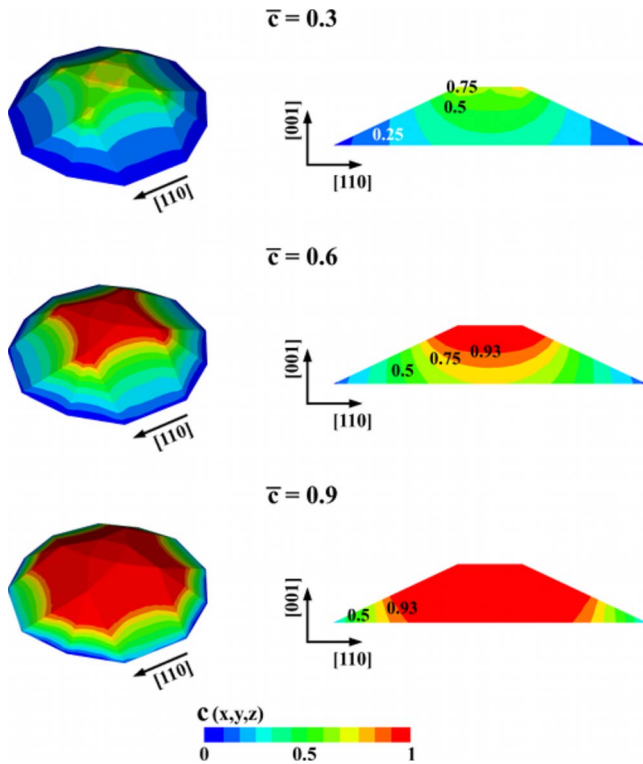


FIG. 7. (Color online) Distribution of Ge minimizing the elastic energy within a dome-shaped island with average Ge content $\bar{c} = 0.3$ (left and right panel at the top), $\bar{c} = 0.6$ (central), and $\bar{c} = 0.9$ (bottom).

$\sim 90\%$, approaching local complete segregation. Finally, at $\bar{c} = 0.9$ a large region of the island is made of pure Ge. A somewhat similar behavior is found for domes (Fig. 7). The concentration gradient is, however, larger, so that local segregation is already appearing around $\bar{c} = 0.6$. The trend is continued by moving to the steepest islands here considered, barns (Fig. 8). In order to understand the above introduced universal behavior, it is convenient to scale the $c_{\min}(x, y, z)$ plots with respect to the average \bar{c} . This is done in Fig. 9 for domes, used as a representative example. Pyramids and barns, indeed, show identical qualitative behavior. From the figure, it is quite evident that the normalized concentration distributions are identical for $\bar{c} = 0.1$ and $\bar{c} = 0.3$. This behavior cannot take place at any \bar{c} value. Typically, the 2.25 isoline must disappear for $\bar{c} \geq 0.45$, otherwise unphysical concentration values would be predicted. Indeed, at $\bar{c} = 0.6$ the higher isolines are expelled from the plot which now appear different. For the even higher $\bar{c} = 0.9$, the plot approaches the fully uniform $\bar{c} = 1$ limit. In other words, it is the onset of local complete segregation which breaks the universal behavior. Starting from a critical \bar{c} , 100% Ge starts appearing, preventing any further scaling. In the curves displayed in Fig. 5 this is signaled by the onset of the quickly increasing portion of the curves yielding the relative energy relaxation with respect to \bar{c} . Since, as shown in Figs. 6–8, the steeper is the island the stronger the driving force leading to segregation, the concentration range where the universal behavior takes place is more extended for pyramids, while rather limited for barns. Interestingly, the typical average concentration

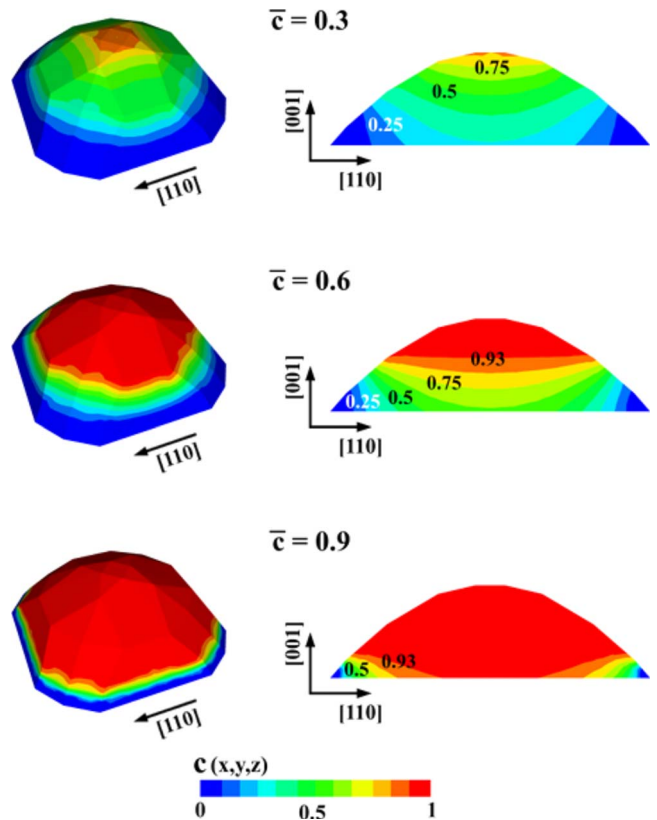


FIG. 8. (Color online) Distribution of Ge minimizing the elastic energy within a barn-shaped island with average Ge content $\bar{c} = 0.3$ (left and right panel at the top), $\bar{c} = 0.6$ (central), and $\bar{c} = 0.9$ (bottom).

values (25–50 %) measured for islands grown at sufficiently high temperatures³⁴ fall within the scalable range, so that a single calculation is sufficient to estimate the lower limit for the elastic energy stored in the island.

Let us now look at the effects of energy minimization on the local elastic-energy distribution both within the island and in the substrate. A single example is shown, since it is sufficient to clarify several general issues. In Fig. 10, the elastic-energy density W is plotted for the same dome island,

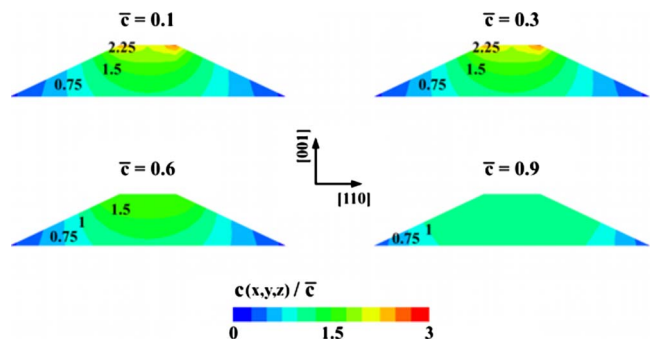


FIG. 9. (Color online) Distribution of Ge minimizing the elastic energy within a dome-shaped island, divided by the average concentration \bar{c} . Top left: $\bar{c} = 0.1$. Top right: $\bar{c} = 0.3$. Bottom left: $\bar{c} = 0.6$. Bottom right: $\bar{c} = 0.9$. Besides using a color scale, a few numerical values are reported.

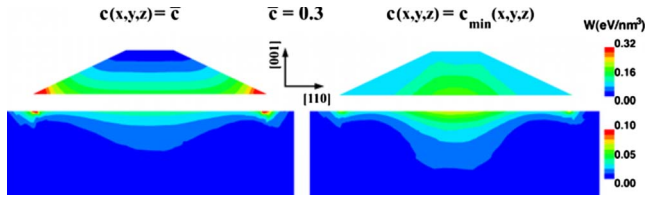


FIG. 10. (Color online) Left: elastic energy density W in the full island + Si-substrate system for a dome island with uniform Ge distribution $c(x,y,z)=0.3$. Right: W for the same island, but with the Ge concentration minimizing the total elastic energy. In both cases, the island is artificially shown as slightly lifted from the substrate. We used this graphical artifact to make more evident that two different color scales (between 0 and 0.32 eV/nm³ for the island, and between 0 and 0.1 eV/nm³ for the substrate) are used to yield a clearer picture. The same scale, instead, is used to treat the uniform and the $c_{\min}(x,y,z)$ case.

and the same average concentration, comparing a uniform distribution with $c_{\min}(x,y,z)$. If the concentration is uniform, the elastic energy is highly non uniform, while if the Ge distribution minimizes the energy (therefore becoming highly non uniform, see Fig. 7) W becomes almost uniform. Notice also the different distribution of the elastic load between island and substrate. If the Ge distribution minimizes the energy, then the island is more relaxed. In order to recover the desired lattice parameter, however, a larger distortion is produced in the substrate where the stored energy is raised with respect to the uniform case. If the uniform case exemplifies the typical base-to-top relaxation, this popular description of the island behavior is lost if the material is able to rearrange following $c_{\min}(x,y,z)$.

A last point deserves some discussion. If in Fig. 10 we showed how the elastic-energy distribution within the island becomes more uniform when Ge is distributed following c_{\min} , there is another relevant quantity which becomes exactly constant provided that \bar{c} is in the universal-behavior range. In Fig. 11, indeed, we report the hydrostatic stress σ_{xyz} (trace of the stress tensor) for the same \bar{c} values analyzed in Fig. 9 in terms of rescaled Ge distribution. For $\bar{c}=0.1$ and $\bar{c}=0.3$, the hydrostatic stress in the island is uniform. Obviously, the absolute value (explicitly reported in the figure) changes, more compression being felt at the higher average concentration. The substrate (not shown), instead, follows the same nonuniform behavior already reported in Fig. 10 for

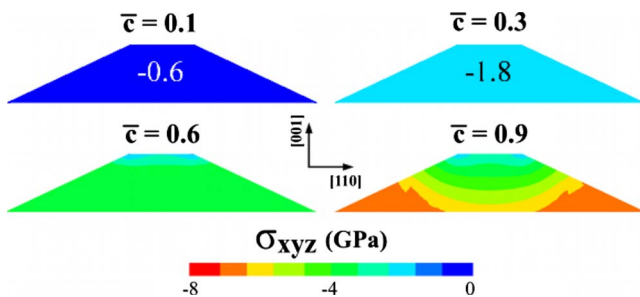


FIG. 11. (Color online) Hydrostatic stress σ_{xyz} for a dome-shaped island, after energy minimization. Four different average concentrations \bar{c} are considered.

the elastic energy. As soon as \bar{c} exceeds the universal behavior range ($\bar{c}=0.6$), so that pure-Ge accumulation at the very top of the island starts developing, a dependence of σ_{xyz} on the position is found, the effect being more pronounced at the higher $\bar{c}=0.9$ value. The constant hydrostatic stress result could have been predicted purely on the basis of Eq. (10). Indeed, exploiting the simple relation⁴⁴ $A[\text{Tr } \epsilon - 3\epsilon_m c] = \text{Tr } \sigma$, one sees that $\text{Tr } \sigma = \text{Tr } \sigma$ if $\Delta c = 0$, i.e., when convergence is reached. Once again, in the derivation of Eq. (10) the constraint $0 \leq c(x,y,z) \leq 1$ is not imposed. If values outside the physical range are predicted by Eq. (10), the regularization procedure described in Sec. IV locally corrects the concentration. Under these conditions the hydrostatic stress does not need to be uniform anymore (Fig. 11).

The constant hydrostatic stress result can be interpreted using a parallelism between our system and a fluid. After all, we assume that the material is able to freely move within the island volume, so that the comparison makes some sense. Starting from Eq. (5), yielding the energy variation accompanying a change in concentration at fixed strain, and considering an infinitesimal variation in concentration δc (leading to an infinitesimal change δE in energy), one can derive the following expression for the chemical potential:

$$\mu \equiv \frac{\delta E}{\delta c} = -\epsilon_m \text{Tr } \sigma. \quad (14)$$

If the Ge distribution minimizes the elastic energy, then the chemical potential has null gradient in the island. In a Fick-equation framework this means that $\vec{j} = -D \vec{\nabla} \mu = 0 = \partial c / \partial t$, where D is the diffusion coefficient, \vec{j} the current, and t the time. The concentration distribution $c_{\min}(x,y,z)$ can be therefore seen as a stationary solution.

VI. DISCUSSION AND CONCLUSIONS

Besides the understanding of the fundamental physics involved in strain relaxation in alloyed systems, and the importance of c_{\min} per se, indicating the most relaxed configuration for a given average concentration, one can ask whether studying the $c_{\min}(x,y,z)$ concentration profiles is of direct usefulness when analyzing experimental data. In determining $c_{\min}(x,y,z)$ we assumed that every Si and Ge atom present in the island is able to move to the energetically more convenient position. Bulk diffusion should hence be active in a real SiGe system in order to allow for the optimal c_{\min} to be observed. Kinetic barriers are, however, way too high to allow for true volumetric rearrangements¹² at the typical experimental temperatures. Beside, if the system evolution was truly driven by thermodynamics, the important role of entropy should be considered,³⁰ leading to Ge distributions much more uniform than the ones here presented. Very interestingly, it looks like the very complex kinetics of SiGe islands grown on Si(001) can lead in some cases to distributions closely resembling c_{\min} . In Ref. 38, indeed, this was demonstrated for a dome with $\bar{c}=0.6$ (also reported here, see Fig. 7), representative of the one experimentally analyzed by selective etching in Ref. 27, after growth at a moderate temperature (580 °C). This surely does not mean that bulk dif-

fusion is activated at 580 °C (even because, as already stressed, with bulk diffusion taking place entropy would determine a profile⁴² very different from the experimental one), and, indeed, a speculative justification purely based on surface (or subsurface) processes can be given. We recall that, during the initial stages of 3D growth, Si is mainly originated from trenches⁵ excavated around the islands to relieve the strong compression present in that region.^{49,51} Trenches, however, do not form immediately and become progressively deeper as the island volume is enlarged,⁵ so that as soon as the island is formed (typically assuming a pyramidal shape, and transforming to dome only in a second stage)^{52–54} a very high Ge content is expected. As soon as Si starts spilling out of trenches, Si-enrichment at island edges is favored both by kinetics (the Si source being close and exchanges with Ge atoms underneath being fast)⁵⁵ and by elastic-energy lowering (Fig. 7). At the same time, also further Ge atoms reach the island, partially relieving strain by intermixing with Si, and partially climbing along the exposed facets and reaching the top regions, which are energetically favored. With this respect, the higher Ge content in the central, internal region of the island could be a reminiscence of the initial stages of formation, the actual profile being caused by the progressive reshaping allowed for by Si/Ge exchanges, limited, however, to the very outermost layers^{12,35} where kinetic barriers are sufficiently low. For islands grown at higher temperatures, instead, it looks like the c_{\min} profile deviates more substantially from the experimental one (compare Fig. 7 with Fig. 2 in Ref. 34 where a dome grown at 740 °C is analyzed), the latter being more uniform. In addition, the justification proposed here for Ge-rich island cores seems not to apply anymore, since in Ref. 34 a very high Si concentration is re-

vealed also in the island interior. Hence, it looks like the development of models capturing both kinetics and thermodynamics is needed to provide comparisons between theory and experiments in the full range of relevant growth temperatures. With this respect, the continuum approach of Tu and Tersoff³² appears as particularly promising, even if limited, so far, to shallow islands in 2D.

In conclusion, by exploiting the fast semianalytical approach proposed in this paper, we have systematically investigated minimum-energy concentration profiles and the corresponding elastic relaxation for different, realistically shaped SiGe islands. We showed that the driving force for nonuniform intermixing grows with the island aspect ratio. Moreover, we pointed out that whenever full segregation is not present within the island (true for small enough average Ge concentration values \bar{c} and/or aspect ratios), a universal behavior is observed. Once the shape is fixed, calculations for a given \bar{c} are sufficient to infer the Ge distribution at any other average concentration value. Equivalently, the extra-relaxation energy with respect to the uniform case, does not depend on \bar{c} .

ACKNOWLEDGMENTS

We acknowledge very fruitful discussions with J. Tersoff, who helped us to work out the parallelism with fluids, and with Leo Miglio who pointed to us the possibility of understanding higher Ge concentration values in the interior of real islands as a result of the first stages of growth, occurring in a richer Ge environment. Financial support by the EU-funded project D-DotFET is also gratefully acknowledged.

*francesco.montalenti@unimib.it

- ¹J. E. Ayers, *Heteroepitaxy of Semiconductors* (CRC press, London, 2007).
- ²I. Berbezier and A. Ronda, *Surf. Sci. Rep.* **64**, 47 (2009).
- ³T. I. Kamins, G. Medeiros-Ribeiro, D. A. A. Ohlberg, and R. S. Williams, *Appl. Phys. A: Mater. Sci. Process.* **67**, 727 (1998).
- ⁴J. Tersoff, *Phys. Rev. Lett.* **81**, 3183 (1998).
- ⁵S. A. Chaparro, J. Drucker, Y. Zhang, D. Chandrasekhar, M. R. McCartney, and D. J. Smith, *Phys. Rev. Lett.* **83**, 1199 (1999).
- ⁶N. Liu, J. Tersoff, O. Baklenov, A. L. Holmes, and C. K. Shih, *Phys. Rev. Lett.* **84**, 334 (2000).
- ⁷F. Boscherini, G. Capellini, L. Di Gaspare, F. Rosei, N. Motta, and S. Mobilio, *Appl. Phys. Lett.* **76**, 682 (2000).
- ⁸I. Kegel, T. H. Metzger, A. Lorke, J. Peisl, J. Stangl, G. Bauer, J. M. García, and P. M. Petroff, *Phys. Rev. Lett.* **85**, 1694 (2000).
- ⁹X. R. Qin, B. S. Swartzentruber, and M. G. Lagally, *Phys. Rev. Lett.* **85**, 3660 (2000).
- ¹⁰S. A. Chaparro, Y. Zhang, J. Drucker, D. Chandrasekhar, and D. J. Smith, *J. Appl. Phys.* **87**, 2245 (2000).
- ¹¹O. G. Schmidt and K. Eberl, *Phys. Rev. B* **61**, 13721 (2000).
- ¹²B. P. Uberuaga, M. Leskovar, A. P. Smith, H. Jónsson, and M. Olmstead, *Phys. Rev. Lett.* **84**, 2441 (2000).
- ¹³X. Z. Liao, J. Zou, D. J. H. Cockayne, Z. M. Jiang, X. Wang, and

R. Leon, *Appl. Phys. Lett.* **77**, 1304 (2000).

- ¹⁴S. A. Chaparro, Y. Zhang, and J. Drucker, *Appl. Phys. Lett.* **76**, 3534 (2000).
- ¹⁵G. Capellini, M. De Seta, and F. Evangelisti, *Appl. Phys. Lett.* **78**, 303 (2001).
- ¹⁶T. Walther, A. G. Cullis, D. J. Norris, and M. Hopkinson, *Phys. Rev. Lett.* **86**, 2381 (2001).
- ¹⁷M. A. Migliorato, A. G. Cullis, M. Fearn, and J. H. Jefferson, *Phys. Rev. B* **65**, 115316 (2002).
- ¹⁸A. Malachias, S. Kycia, G. Medeiros-Ribeiro, R. Magalhães-Paniago, T. I. Kamins, and R. S. Williams, *Phys. Rev. Lett.* **91**, 176101 (2003).
- ¹⁹U. Denker, H. Sigg, and O. G. Schmidt, *Appl. Surf. Sci.* **224**, 127 (2004).
- ²⁰R. J. Wagner and E. Gulari, *Phys. Rev. B* **69**, 195312 (2004).
- ²¹G. Medeiros-Ribeiro, A. Malachias, S. Kycia, R. Magalhães-Paniago, T. I. Kamins, and R. S. Williams, *Appl. Phys. A: Mater. Sci. Process.* **80**, 1211 (2005).
- ²²U. Denker, A. Rastelli, M. Stoffel, J. Tersoff, G. Katsaros, G. Costantini, K. Kern, N. Y. Jin-Phillip, D. E. Jesson, and O. G. Schmidt, *Phys. Rev. Lett.* **94**, 216103 (2005).
- ²³G. Hadjisavvas and P. C. Kelires, *Phys. Rev. B* **72**, 075334 (2005).

- ²⁴C. Lang, D. J. H. Cockayne, and D. Nguyen-Manh, *Phys. Rev. B* **72**, 155328 (2005).
- ²⁵B. J. Spencer and M. Blaniariu, *Phys. Rev. Lett.* **95**, 206101 (2005).
- ²⁶M. Stoffel, A. Rastelli, S. Kiravittaya, and O. G. Schmidt, *Phys. Rev. B* **72**, 205411 (2005).
- ²⁷G. Katsaros, G. Costantini, M. Stoffel, R. Esteban, A. M. Bittner, A. Rastelli, U. Denker, O. G. Schmidt, and K. Kern, *Phys. Rev. B* **72**, 195320 (2005).
- ²⁸T. U. Schüllli, M.-I. Richard, G. Renaud, V. Favre-Nicolin, E. Wintersberger, and G. Bauer, *Appl. Phys. Lett.* **89**, 143114 (2006).
- ²⁹F. Ratto, G. Costantini, A. Rastelli, O. G. Schmidt, K. Kern, and F. Rosei, *J. Exp. Nanosci.* **1**, 279 (2006).
- ³⁰G. Medeiros-Ribeiro and R. S. Williams, *Nano Lett.* **7**, 223 (2007).
- ³¹G. Katsaros, M. Stoffel, A. Rastelli, O. G. Schmidt, K. Kern, and J. Tersoff, *Appl. Phys. Lett.* **91**, 013112 (2007).
- ³²Y. Tu and J. Tersoff, *Phys. Rev. Lett.* **98**, 096103 (2007).
- ³³M. S. Leite, G. Medeiros-Ribeiro, T. I. Kamins, and R. S. Williams, *Phys. Rev. Lett.* **98**, 165901 (2007).
- ³⁴A. Rastelli, M. Stoffel, A. Malachias, T. Merdzhanova, G. Katsaros, K. Kern, T. H. Metzger, and O. G. Schmidt, *Nano Lett.* **8**, 1404 (2008).
- ³⁵F. Zipoli, S. Cereda, M. Ceriotti, M. Bernasconi, L. Miglio, and F. Montalenti, *Appl. Phys. Lett.* **92**, 191908 (2008).
- ³⁶N. V. Medhekar, V. Hegadekatte, and V. B. Shenoy, *Phys. Rev. Lett.* **100**, 106104 (2008).
- ³⁷M. S. Leite, A. Malachias, S. W. Kycia, T. I. Kamins, R. S. Williams, and G. Medeiros-Ribeiro, *Phys. Rev. Lett.* **100**, 226101 (2008).
- ³⁸R. Gatti, F. Uhlík, and F. Montalenti, *New J. Phys.* **10**, 083039 (2008).
- ³⁹A. Rastelli, M. Stoffel, T. Merdzhanova, and O. G. Schmidt, *J. Phys.: Condens. Matter* **20**, 454214 (2008).
- ⁴⁰T. U. Schüllli, G. Vastola, M.-I. Richard, A. Malachias, G. Renaud, F. Uhlík, F. Montalenti, G. Chen, L. Miglio, F. Schäfler, and G. Bauer, *Phys. Rev. Lett.* **102**, 025502 (2009).
- ⁴¹M. S. Leite, T. I. Kamins, and G. Medeiros-Ribeiro, *Appl. Phys. Lett.* **94**, 053118 (2009).
- ⁴²F. Uhlík, R. Gatti, and F. Montalenti, *J. Phys.: Condens. Matter* **21**, 084217 (2009).
- ⁴³Rob Phillips, *Crystals, Defects and Microstructures* (Cambridge University Press, Cambridge, England, 2001).
- ⁴⁴J. D. Eshelby, *Proc. R. Soc. London, Ser. A* **241**, 376 (1957).
- ⁴⁵In this work, we used the commercial COMSOL MULTIPHYSICS package as a FEM solver.
- ⁴⁶*Handbook of Chemistry and Physics*, edited by D. R. Lide (CRC press, Boca Raton, FL, 2007).
- ⁴⁷In Fig. 3, one can notice the sharp angle formed between the $M=10$ curve and the standard MC-FEM value. Sharper angles are obtained for larger M . This feature is simply due to the straight application of our algorithm which calls FEM only after M accepted moves. This means that $(M-1)$ moves before the theoretical convergence, the iterative procedure is stopped. For large M values this would lead to a non-negligible deviation from the correct result. This problem can be fixed by simply reducing M on the fly during the simulation, e.g., based on the acceptance ratio. We did not discuss this procedure in the text since, at the end, results are obtained using the faster method of Sec. IV.
- ⁴⁸A. Marzegalli, V. A. Zinovyev, F. Montalenti, A. Rastelli, M. Stoffel, T. Merdzhanova, O. G. Schmidt, and L. Miglio, *Phys. Rev. Lett.* **99**, 235505 (2007).
- ⁴⁹*Self-Assembled Quantum Dots*, edited by Z. M. Wang (Springer, Berlin, 2008), Chap. 14.
- ⁵⁰In principle, one should consider position-dependent elastic constants determined by the local concentration value. While we did work out the required generalization of Eq. (10), the formalism becomes rather complex. Since we verified that results negligibly deviate from the \bar{c} -dependent anisotropic constants choice, which, in turn, yields concentration profiles very close to the even simpler pure-Ge constants case, we shall keep the notation light, without reporting the above generalization. For heteroepitaxial systems, where the difference in elastic constants between the two materials is larger, the extension might be needed.
- ⁵¹D. T. Tambe and V. B. Shenoy, *Appl. Phys. Lett.* **85**, 1586 (2004).
- ⁵²G. Medeiros-Ribeiro, A. Bratkovski, T. I. Kamins, D. A. A. Ohlberg, and R. S. Williams, *Science* **279**, 353 (1998).
- ⁵³F. M. Ross, R. M. Tromp, and M. C. Reuter, *Science* **286**, 1931 (1999).
- ⁵⁴F. Montalenti, P. Raiteri, D. B. Migas, H. von Känel, A. Rastelli, C. Manzano, G. Costantini, U. Denker, O. G. Schmidt, K. Kern, and L. Miglio, *Phys. Rev. Lett.* **93**, 216102 (2004).
- ⁵⁵S. Cereda and F. Montalenti (unpublished).